

Metabolic labeling enables selective photocrosslinking of O-GlcNAc-modified proteins to their binding partners

Seok-Ho Yu^a, Michael Boyce^b, Amberlyn M. Wands^a, Michelle R. Bond^a, Carolyn R. Bertozzi^b, and Jennifer J. Kohler^{a,1}

^aDepartment of Biochemistry, University of Texas Southwestern Medical Center, Dallas, TX 75390-9038 and ^bDepartment of Chemistry, University of California, Berkeley, CA 94720

Edited by Barbara Imperiali, Massachusetts Institute of Technology, Cambridge, MA, and approved January 30, 2012 (received for review August 31, 2011)

O-linked β -*N*-acetylglucosamine (O-GlcNAc) is a reversible post-translational modification found on hundreds of nuclear and cytoplasmic proteins in higher eukaryotes. Despite its ubiquity and essentiality in mammals, functional roles for the O-GlcNAc modification remain poorly defined. Here we develop a combined genetic and chemical approach that enables introduction of the diazirine photocrosslinker onto the O-GlcNAc modification in cells. We engineered mammalian cells to produce diazirine-modified O-GlcNAc by expressing a mutant form of UDP-GlcNAc pyrophosphorylase and subsequently culturing these cells with a cell-permeable, diazirine-modified form of GlcNAc-1-phosphate. Irradiation of cells with UV light activated the crosslinker, resulting in formation of covalent bonds between O-GlcNAc-modified proteins and neighboring molecules, which could be identified by mass spectrometry. We used this method to identify interaction partners for the O-GlcNAc-modified FG-repeat nucleoporins. We observed crosslinking between FG-repeat nucleoporins and nuclear transport factors, suggesting that O-GlcNAc residues are intimately associated with essential recognition events in nuclear transport. Further, we propose that the method reported here could find widespread use in investigating the functional consequences of O-GlcNAcylation.

diazirine | glycosylation | metabolism | nucleoporins | posttranslational modification

O-linked β -*N*-acetylglucosamine (O-GlcNAc) is a common modification of intracellular proteins in metazoa and higher plants (1). Hundreds of O-GlcNAc-modified human nuclear and cytoplasmic proteins have been identified. Modified proteins fall into a variety of functional classes and include transcription factors, ribosomal proteins and translational factors, signaling proteins, cytoskeletal proteins, and components of the nuclear pore complex. Like phosphorylation, O-GlcNAcylation is reversible. Mammalian genomes encode a single O-GlcNAc transferase (OGT) that transfers GlcNAc from the nucleotide sugar donor UDP-GlcNAc to serine or threonine side chains of substrate proteins, and one O-GlcNAcase (nuclear cytoplasmic O-GlcNAcase and acetyltransferase; NCOAT) that hydrolytically removes GlcNAc residues from modified proteins. The O-GlcNAc modification is essential in mammals (2) and O-GlcNAc is critical to cells' ability to tolerate a variety of forms of stress (3, 4).

While characterization of O-GlcNAc-modification sites has advanced dramatically (5), a comprehensive understanding of the functional consequences of O-GlcNAc modification remains more elusive (6). How does O-GlcNAc affect a protein's activity, stability, and ability to engage in binding interactions? O-GlcNAc is often found at sites that can be alternatively phosphorylated, leading to a reciprocal relationship between these two modifications. This relationship led to the hypothesis that a key role for O-GlcNAc is to interfere with phosphorylation (7). In fact, experimental evidence suggests that the interplay between these two modifications is complex, involving both negative and positive associations (8–10). Another documented function for O-GlcNAc is to disrupt binding interactions of the modified proteins, presumably by steric interference (11). Less clear is whether the O-GlcNAc modification can impart a novel activity to the

modified protein, although recent findings suggest that increased levels of O-GlcNAc can be associated with acquisition of function (12–14).

Selectively observing the cellular behavior of O-GlcNAc-modified proteins remains challenging. Most methods report on the bulk behavior of the protein of interest and do not distinguish among the different posttranslationally modified forms. We reasoned that appending a small photoactivatable crosslinking group to the O-GlcNAc modification would enable selectively induced covalent crosslinking between an O-GlcNAc-modified protein and surrounding molecules. Because the crosslinker is on the O-GlcNAc residue, proteins that lack the modification will not engage in crosslinking and will be rendered essentially invisible in this assay. In this way, even proteins that are O-GlcNAc-modified at substoichiometric levels could be examined.

To implement the photocrosslinking approach, we designed an analog of GlcNAc, GlcNDAz, in which the *N*-acyl substituent was modified to include the diazirine photocrosslinker (Fig. 1). Using a metabolic labeling approach, we induced cultured cells to produce the modified nucleotide sugar donor UDP-GlcNDAz and to transfer GlcNDAz to proteins that are normally O-GlcNAc-modified. Subsequent photoirradiation resulted in the selective covalent crosslinking of O-GlcNDAz-modified proteins. Mass spectrometry analysis of purified complexes revealed crosslinking between O-GlcNAc-modified nucleoporins and nuclear transport factors. These results indicate that the O-GlcNAc modification is intimately associated with the recognition events that occur during nuclear transport.

Results

In Vitro Production and Crosslinking of O-GlcNDAz-modified Peptides.

We envisioned that introduction of a photocrosslinking group directly onto an O-GlcNAc residue would enable the covalent crosslinking between the O-GlcNAc modification and proximal molecules. To test this idea, we assessed crosslinking between an O-GlcNDAz-modified peptide and a monoclonal antibody, RL2 (15), that specifically recognizes the O-GlcNAc modification. First, we prepared the diazirine-modified nucleotide-sugar donor UDP-GlcNDAz (Fig. 1) (16) and incubated it with recombinant human OGT and a biotinylated substrate peptide derived from casein kinase II (CKII) (17). The product mixture was analyzed by MALDI mass spectrometry, revealing a mass consistent with transfer of the GlcNDAz residue to the CKII peptide (Fig. S14). Next, the O-GlcNDAz-modified peptide was incubated with RL2 and UV irradiated to induce photocrosslinking (Fig. S24).

Author contributions: S.-H.Y., M.B., C.R.B., and J.J.K. designed research; S.-H.Y. and M.B. performed research; S.-H.Y., A.M.W., and M.R.B. contributed new reagents/analytic tools; S.-H.Y., M.B., C.R.B., and J.J.K. analyzed data; and S.-H.Y., M.B., C.R.B., and J.J.K. wrote the paper.

The authors declare no conflict of interest.

This article is a PNAS Direct Submission.

¹To whom correspondence should be addressed: E-mail: jennifer.kohler@utsouthwestern.edu.

This article contains supporting information online at www.pnas.org/lookup/suppl/doi:10.1073/pnas.1114356109/-DCSupplemental.

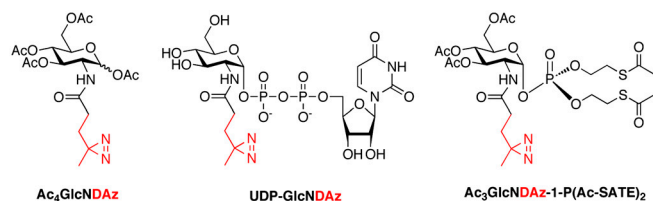


Fig. 1. Diazirine-modified GlcNAc derivatives used in this study.

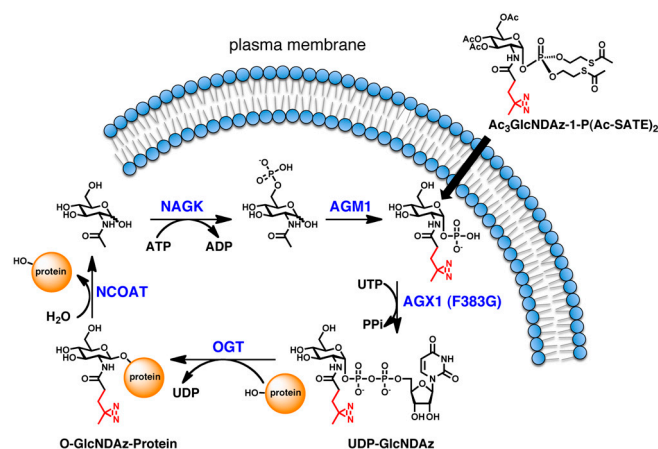


Fig. 2. Metabolic labeling strategy for cellular biosynthesis of O-GlcNDAz-modified proteins. Cellular GlcNAc can be converted to UDP-GlcNDAz via three enzymatic steps catalyzed by *N*-acetylglucosamine kinase (NAGK), *N*-acetylglucosamine-phosphate mutase (AGM1), and UDP-GlcNAc pyrophosphorylase (AGX1 or AGX2). HeLa cells expressing AGX1(F383G) and cultured with Ac₃GlcNDAz-1-P(Ac-SATE)₂ efficiently produced UDP-GlcNDAz.

Immunoblot analysis revealed a biotinylated species migrating with an apparent molecular weight identical to that of the light chain of RL2 (Fig. S2B). Observation of the biotinylated species depended on inclusion of the crosslinker (UDP-GlcNDAz) and on UV irradiation. We concluded that this biotinylated species represented the O-GlcNDAz-modified peptide crosslinked to the light chain of the RL2 antibody. These results indicate that the addition of the diazirine modification to GlcNAc does not preclude transfer of the sugar by OGT nor does it abrogate the binding interaction between O-GlcNAc-modified CKII and RL2.

Having established that human OGT is capable of accepting UDP-GlcNDAz, we conducted competition experiments to determine whether OGT would transfer GlcNDAz from UDP-GlcNDAz when UDP-GlcNAc was also available. Lysates prepared from HeLa cells overexpressing human OGT were incubated with UDP-GlcNAc, UDP-GlcNDAz or an equimolar mixture of the two, along with an OGT acceptor peptide (+P2) derived from human α -A crystallin (18) (Fig. S1B). Lysates incubated with UDP-GlcNAc produced a product with the mass ($m/z = 1,241$) expected for an O-GlcNAc-modified peptide. Lysates incubated with UDP-GlcNDAz produced a product whose mass corresponded to the intact O-GlcNDAz-modified peptide ($m/z = 1,309$) and an additional product whose mass was consistent with loss of N₂ from the O-GlcNDAz-modified peptide ($m/z = 1,281$). Loss of N₂ likely occurs during the mass spectrometry ionization step, a phenomenon we have observed with other diazirine-containing molecules (19). When OGT-containing lysates were incubated with an equimolar mixture of UDP-GlcNAc and UDP-GlcNDAz, masses corresponding to both O-GlcNAc- and O-GlcNDAz-modified peptides were observed. We repeated the experiment with recombinant OGT, rather than lysate, and analyzed the peptide products by HPLC. The O-GlcNAc-modified peptide was the major product (Fig. S1C), but the O-GlcNDAz-modified peptide was also observed. While these data indicate that OGT prefers UDP-GlcNAc over UDP-GlcNDAz, the O-GlcNDAz-modified peptide was readily produced when the two nucleotide sugars were present in comparable amounts.

Cellular Production of UDP-GlcNDAz. We next focused attention on engineering cells to produce UDP-GlcNDAz, so that O-GlcNDAz-modified proteins could be produced in cells (Fig. 2). In mammalian cells, UDP-GlcNAc can be produced from GlcNAc through three enzymatic steps of the GlcNAc salvage pathway. Hoping to take advantage of the endogenous pathway, we prepared a peracetylated form of GlcNDAz, Ac₄GlcNDAz, and added it to the media of cultured cells to test whether the cells could convert this compound to UDP-GlcNDAz. We used high performance anion exchange chromatography (HPAEC) analysis of the lysates to assess UDP-GlcNDAz production in multiple cell lines (HeLa, Jurkat, BJAB K20), but could not detect the photocrosslinking nucleotide sugar (UDP-GlcNDAz). We also failed to observe production of GlcNDAz-1-P, suggesting inadequate conversion by either *N*-acetylglucosamine kinase (NAGK), which phosphorylates GlcNAc at C6, or *N*-acetylglucosamine-phosphate mutase (AGM1), which converts GlcNAc-6-P to GlcNAc-1-P. To circumvent this metabolic restriction, we prepared a form of GlcNDAz-1-P in which the hydroxyl groups are peracetylated and the phos-

phate is protected with two S-acetyl-2-thioethyl (Ac-SATE) groups. We predicted that Ac₃GlcNDAz-1-P(Ac-SATE)₂ would be capable of diffusing across the plasma membrane, after which the protecting groups would be removed by chemical hydrolysis or the action of intracellular esterases (20). Indeed, HPAEC analysis of HeLa lysates revealed that cells cultured with Ac₃GlcNDAz-1-P(Ac-SATE)₂ readily accumulated intracellular GlcNDAz-1-P; however, UDP-GlcNDAz was not detected (Fig. S3A). These data suggested that GlcNDAz-1-P is a poor substrate for AGX1 and/or AGX2, the two splice variant isoforms of UDP-GlcNAc pyrophosphorylase.

Examination of the X-ray crystal structure of human AGX1 (PDB code 1JV1) (21) revealed that the *N*-acetyl group of the bound UDP-GlcNAc resides in a compact hydrophobic pocket bounded by two phenylalanine residues (Fig. 3A; F381 and F383). We hypothesized that the hydrophobic pocket was too small to accommodate the *N*-acyl diazirine substituent and designed mutants of AGX1 (F381G and F383G) predicted to have expanded binding pockets. HeLa cells were transiently transfected with plasmids encoding wild-type AGX1, AGX1(F381G), or AGX1(F383G), and cultured in media containing Ac₃GlcNDAz-1-P(Ac-SATE)₂. HPAEC analysis of the lysates showed that cells transfected with mutant AGX1(F383G) efficiently produced a metabolite whose mobility matched that of synthetic UDP-GlcNDAz (Fig. 3B). The identity of UDP-GlcNDAz was confirmed by UV irradiating both the lysate and the UDP-GlcNDAz standard compound and comparing their HPAEC patterns (Fig. S3B). In addition, the UDP-GlcNDAz peak from the AGX1(F383G)-expressing lysate was collected and analyzed by MALDI-TOF mass spectrometry, revealing the expected mass (Fig. S3C). HeLa cells transfected with wild-type AGX1 did not produce UDP-GlcNDAz, indicating that UDP-GlcNDAz production was not simply due to AGX1 overexpression (Fig. 3B). Furthermore, UDP-GlcNDAz production occurs in a time-dependent manner (Fig. S3D). Thus, expression of AGX1(F383G) permits conversion of GlcNDAz-1-P to UDP-GlcNDAz in cells, likely by expanding the enzyme's binding pocket to accommodate the unnatural sugar. Notably, cells expressing AGX1(F383G) and cultured in media containing Ac₄GlcNDAz did not produce UDP-GlcNDAz, confirming that conversion of GlcNDAz to GlcNDAz-1-P is inefficient (Fig. S3E).

Cellular Production of O-GlcNDAz-modified proteins. We wished to investigate whether HeLa cells producing UDP-GlcNDAz could incorporate GlcNDAz into O-GlcNDAz-modified proteins. We

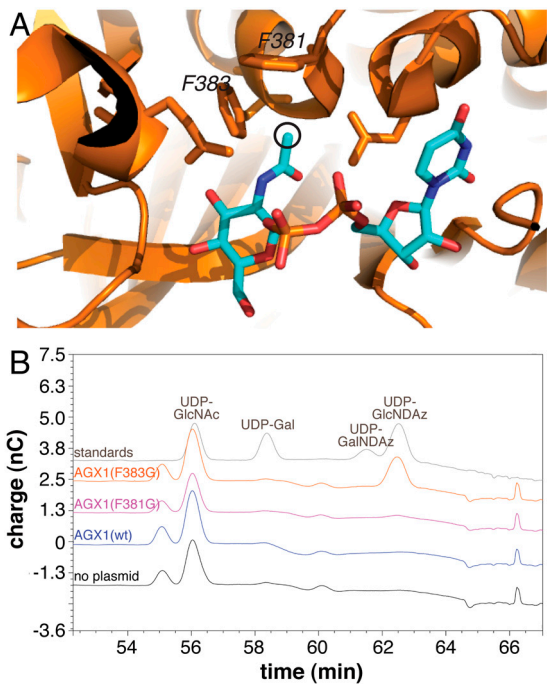


Fig. 3. Structure-guided mutagenesis of AGX1 results in efficient UDP-GlcNAz production. (A) The X-ray crystal structure of human AGX1 (PDB code 1JV1)(21) reveals that F381 and F383 surround the *N*-acetyl group of UDP-GlcNAc. Black circle indicates position where the unnatural alkyl diazirine substituent is attached in UDP-GlcNAz. (B) HPAEC-PAD analysis of lysates from HeLa cells transiently transfected with DNA encoding wild-type AGX1, AGX1(F381G), AGX1(F383G), or no vector and cultured with Ac₃GlcNAz-1-P(Ac-SATE)₂. Chromatogram of standard nucleotide sugars is shown at the top.

reasoned that UV irradiation would result in covalent conjugation of the O-GlcNAz-modified proteins to neighboring molecules. Thus, irradiation of an O-GlcNAz-modified protein should increase the protein's apparent molecular weight, as assessed by immunoblot analysis. To test this idea, we examined the known interaction between O-GlcNAc-modified proteins and the O-GlcNAc-recognizing antibody, RL2. We transfected HeLa cells with AGX1(F383G) and cultured them in media containing Ac₃GlcNAz-1-P(Ac-SATE)₂. Cell lysates were incubated with RL2. After UV irradiation, RL2 was precipitated by protein G beads. The elute from the beads was analyzed by immunoblot, using antibodies that recognize two known O-GlcNAc-modified proteins, transcription factor SP1 and nucleoporin NUP153 (Fig. S4). In both cases, we observed distinct higher molecular weight complexes only when the cells were both transfected with AGX1(F383G) and cultured in media containing Ac₃GlcNAz-1-P(Ac-SATE)₂. This result strongly suggested that the cells produce O-GlcNAz-modified proteins and that O-GlcNAz-modified proteins can be selectively photocrosslinked to neighboring molecules.

Next, we investigated whether O-GlcNAz-modified proteins could be crosslinked to endogenous binding partners in live cells. Again, HeLa cells expressing AGX1(F383G) were cultured with Ac₃GlcNAz-1-P(Ac-SATE)₂. Cultured cells were irradiated, lysed, and analyzed by immunoblot using mAb414, which recognizes nucleoporins containing phenylalanine-glycine (FG) repeats, including NUP62, NUP153, NUP214, NUP358 (Fig. S5A). In addition to bands corresponding to the nucleoporins, additional mAb414 reactivity at higher molecular weights was observed only when cells were transfected with AGX1(F383G) and cultured with Ac₃GlcNAz-1-P(Ac-SATE)₂. Adding Ac₃GlcNAz-1-P(Ac-SATE)₂ at two separate time points enhanced formation of the crosslinked species. While the higher

molecular weight species on the mAb414 immunoblot were not well resolved, distinct photocrosslinked complexes could be observed by probing with antibodies specific for an individual nucleoporin, NUP153 (Fig. 4A) or NUP62 (Fig. S5B). Taken together, these results support the idea that crosslinking is occurring through a diazirine-modified O-GlcNAc residue. In addition, we found similar effects on nucleoporin crosslinking when we introduced AGX1(F383G) and Ac₃GlcNAz-1-P(Ac-SATE)₂ into T84 intestinal epithelial cells (Fig. S5C and S5D), indicating that the engineering strategy is not cell line-specific.

FG-repeat Nucleoporins Interact with Nuclear Transport Factors. Our next goal was to identify proteins that were covalently conjugated to FG-repeat nucleoporins via O-GlcNAz directed crosslinking. To accomplish this, we prepared HeLa cells that stably expressed AGX1(F383G) and cultured the cells with Ac₃GlcNAz-1-P(Ac-SATE)₂. These UDP-GlcNAz-producing cells were UV irradiated and lysed. We conducted an immunoprecipitation of the lysate using mAb414. The immunoprecipitate was separated by SDS-PAGE and visualized by silver-staining (Fig. 4B). The banding pattern was compared to an identical lysate that was not UV irradiated. We identified molecular weight ranges in which significant silver staining was observed in the UV-irradiated sample, but not the nonirradiated sample. These regions were excised from the gel and subjected to in-gel trypsin digest, followed by high performance liquid chromatography tandem mass spectrometry (HPLC/MS/MS) analysis to identify tryptic peptides. The Mascot search engine was used to analyze the mass spectrometry data and develop a candidate list of proteins present in the immunoprecipitate (Table S1). As expected, the putative cross-linked regions contained nucleoporins recognized by mAb414: NUP153, NUP214, and NUP358. In addition, peptides corresponding to several known nuclear transport factors were identified: exportin-1 (CRM1), transportin-1 (TNPO1), transportin-2 (TNPO2), importin subunit β1 (KPNB1), and nuclear RNA export factor 1 (NXF1). The remaining lower confidence hits also corresponded to proteins (histone 2B and γ-catenin) known to enter the nucleus.

To validate the mass spectrometry data, we used a reciprocal immunoprecipitation strategy. UDP-GlcNAz-producing HeLa cells were UV irradiated, then lysed and immunoprecipitated with an anti-TNPO1 antibody to isolate TNPO1 along with any covalent complexes that contained TNPO1. The immunoprecipitate was analyzed by immunoblot using mAb414, as well as antibodies specific for the individual nucleoporins, NUP153,

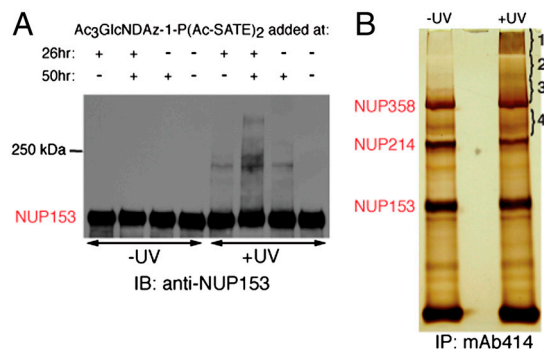


Fig. 4. FG-repeat nucleoporins are crosslinked through O-GlcNAz residues. (A) HeLa cells transiently expressing AGX1(F383G) were cultured with Ac₃GlcNAz-1-P(Ac-SATE)₂ (added 26 and/or 50 h after transfection). Cells were irradiated with 365 nm light, then lysed. Lysates were analyzed by immunoblot using a rabbit anti-NUP153 antibody. (B) HeLa cells stably expressing AGX1(F383G) were cultured with Ac₃GlcNAz-1-P(Ac-SATE)₂. Irradiated and nonirradiated cells were lysed and lysates were immunoprecipitated with mAb414. Immunoprecipitates were separated by SDS-PAGE and visualized by silver staining. Indicated regions of the UV-irradiated sample were analyzed by mass spectrometry.

NUP214, and NUP358. As predicted, the NUP153 and NUP358 antibodies each recognized a higher molecular weight species, consistent with crosslinking between TNPO1 and the nucleoporins. In addition, mAb414 recognized two high molecular weight species, whose apparent molecular weights matched those of the putative crosslinked complexes recognized by anti-NUP153 and anti-NUP358 (Fig. 5). Further confirmation of TNPO1 crosslinking to NUP358 came from a reverse immunoprecipitation experiment. We immunoprecipitated the crosslinked HeLa cell lysate with anti-NUP358 and analyzed the immunoprecipitate with anti-TNPO1 immunoblotting. The anti-NUP358 immunoprecipitate showed clear evidence of a covalent TNPO1-NUP358 complex (Fig. 5, *Right*). Taken together, these results demonstrate that FG-repeat nucleoporins (namely NUP358 and likely NUP153) engage in interactions with the nuclear transport factor TNPO1 and that an O-GlcNAc residue is located at or near to the interaction site. We did not obtain evidence for crosslinking between TNPO1 and NUP214, which could reflect a lack of interaction between these two proteins or the fact that NUP214 crosslinked complexes were poorly visualized on the immunoblot (see input lanes in Fig. 5).

Effects on O-GlcNAc Metabolism. Our metabolic labeling method relies on the introduction of an unnatural metabolite, Ac₃GlcNDAz-1-P(Ac-SATE)₂, and the overexpression of a mutant form of a metabolic enzyme, AGX1. Thus, we were concerned that this strategy could result in perturbations to the normal O-GlcNAc patterns in the cell. Cells stably transfected with the AGX1(F383G)-encoding plasmid produced dramatically increased levels of AGX1 (Fig. S6A), which might be expected to lead to an increased pool of UDP-GlcNAc/UDP-GlcNDAz. We found that the effect of AGX1(F383G) overexpression on the UDP-GlcNAc level was slight (Fig. 3B), although AGX1(F383G) overexpression does lead to the added appearance of UDP-GlcNDAz. Overall, the amount of UDP-GlcNAc/UDP-GlcNDAz in the engineered cells is about twofold higher than the amount of UDP-GlcNAc in normal cells.

We also examined whether NCOAT, the hydrolytic enzyme that removes O-GlcNAc, was capable of recognizing diazirine-modified sugar. We prepared lysates from normal HeLa cells and from HeLa cells transiently transfected with a plasmid encoding NCOAT. These lysates were incubated with artificial substrates, *p*-nitrophenyl-β-D-GlcNAc (pNP-GlcNAc) or *p*-nitrophenyl-β-D-GlcNDAz (pNP-GlcNDAz). We observed significant hydrolysis of pNP-GlcNAc, which dramatically increased with NCOAT overexpression, while hydrolysis of pNP-GlcNDAz was barely detectable with either lysate (Fig. S7). This result implies that O-GlcNDAz residues are resistant to removal by NCOAT and suggests that O-GlcNDAz-modified proteins likely accumulate in cells. Despite effects on the UDP-GlcNAc/UDP-GlcNDAz pool and the resistance of O-GlcNDAz to NCOAT removal, when we probed the lysates from HeLa cells expressing AGX1(F383G) and

cultured with Ac₃GlcNDAz-1-P(Ac-SATE)₂ using RL2, we saw no significant alterations in O-GlcNAcylation (Fig. S6B). This result suggests that our metabolic labeling method does not dramatically perturb the normal O-GlcNAcylation pattern in these cells.

Discussion

We describe a metabolic engineering approach to selectively incorporate crosslinkers into O-GlcNAc residues on nuclear and cytoplasmic proteins. Our initial, *in vitro* experiments demonstrated that a diazirine-modified form of GlcNAc could be transferred by OGT and recognized by an O-GlcNAc-specific antibody, RL2. These results indicated that the relatively small diazirine modification did not abrogate GlcNAc recognition by OGT or by RL2. The ability of OGT to tolerate *N*-acyl modifications to GlcNAc has been shown previously (22) and is consistent with modeling of the OGT-UDP-GlcNAc complex based on the recently reported OGT structure (23).

To incorporate GlcNDAz into O-GlcNAc-modified proteins, we initially hoped to exploit the GlcNAc salvage pathway. However, we discovered at least two metabolic barriers to the conversion of GlcNDAz to UDP-GlcNDAz. First, GlcNDAz is not efficiently converted to GlcNDAz-1-P. We did not conduct experiments to distinguish whether the metabolic barrier is at the phosphorylation step that produces 6-phosphosugar, or in the mutase reaction that converts the 6-phosphosugar to the 1-phosphosugar (or both). Instead, we bypassed the initial barrier by directly delivering a protected form of GlcNDAz-1-P to cells. The second barrier occurs in the pyrophosphorylase step that converts the 1-phosphosugar to the UDP-sugar. Here we used structure-guided mutagenesis to produce a mutant form of AGX1 that tolerates the diazirine modification. Thus, using an approach that combines chemistry and genetic engineering, we induced mammalian cells to produce both UDP-GlcNDAz and O-GlcNDAz-modified proteins. Normally, the O-GlcNAc modification is removed from proteins through the action of the O-GlcNAcase, NCOAT. We found that NCOAT had reduced activity toward an artificial GlcNDAz-containing substrate, suggesting that, in cells, the O-GlcNDAz modification could be more long-lived than O-GlcNAc, and could even be effectively permanent. Thus, our method may cause some perturbations to normal O-GlcNAc patterns, even though no dramatic differences were observed (Fig. S6B).

Metabolic barriers to metabolism of hexosamine analogs have also been observed in efforts to incorporate chemical reporters into O-GlcNAc-modified proteins. An azide-modified GlcNAc analog, GlcNAz, was inefficiently metabolized to the corresponding UDP-GlcNAc analog in 293T cells, but AGX2 overexpression enabled UDP-GlcNAz production, suggesting the presence of only a single metabolic barrier (24). This same report demonstrated that the metabolic barrier could be circumvented by providing cells with an azide-modified GalNAc analog (GalNAz) that was efficiently metabolized to UDP-GalNAz, and further converted to UDP-GlcNAz by the action of the UDP-galactose 4'-epimerase (GALE). More recently, Pratt and coworkers examined metabolism of both azide-modified hexosamines and their alkyne-modified counterparts (25). Their results confirmed the metabolic interconversion of azido-sugars, but indicated that the alkyne-sugars did not efficiently interconvert. Similar to the alkyne case, we did not observe any production of UDP-GalNDAz in our experiments, suggesting that GALE may not readily interconvert the larger, diazirine-modified UDP-sugars. Thus, the hexosamine salvage pathway appears to be sensitive to the exact nature of the *N*-acyl modification and metabolism of any novel analog should be examined carefully. For the experiments described here, the lack of UDP-GalNDAz production is desirable since it is expected to yield more selective incorporation of the diazirine into only GlcNAc-containing glycans.

We demonstrated the utility of O-GlcNDAz crosslinking by using this technique to covalently crosslink nuclear pore proteins

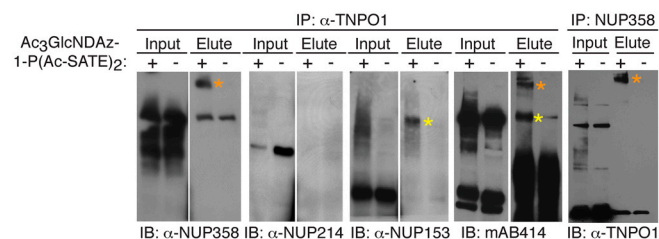


Fig. 5. Transportin-1 interacts with NUP153 and NUP358. HeLa cells stably expressing AGX1(F383G) were cultured with or without Ac₃GlcNDAz-1-P(Ac-SATE)₂. After UV irradiation, the cells were lysed and the lysates were immunoprecipitated with the indicated antibodies. Input lysates and immunoprecipitates were analyzed by immunoblots, as indicated. Two distinct crosslinked species were identified: NUP358-TNPO1 (orange asterisk) and NUP153-TNPO1 (yellow asterisk).

and nuclear transport factors. The mammalian nuclear pore is a 120 MDa complex assembled from about 30 different nucleoporins, each present in multiple copies (26). Transport in and out of the nucleus is regulated by the pore complex: small molecules can diffuse through the pore, while larger molecules are escorted through by karyopherins (27). Karyopherin-cargo complexes translocate through the center of the pore by a poorly understood mechanism that likely involves interactions between karyopherins and the unstructured, FG-repeat nucleoporins that project into the pore. In metazoa, FG-repeat nucleoporins are highly O-GlcNAc-modified, but the functional significance of these modifications has remained unclear. Early work showed that wheat germ agglutinin (WGA), which binds O-GlcNAc, can block transport through the nuclear pore (28), but this finding may reflect the steric bulk of WGA rather than a specific role for O-GlcNAc. More recently, experiments conducted in *Caenorhabditis elegans* offered an opportunity to investigate the significance of the O-GlcNAc modification, since loss of *ogt-1* (the *C. elegans* ortholog of OGT) is not lethal. Hanover and coworkers examined the behavior of several transcription factors in the *ogt-1* deletion strain and found that neither their nuclear localization nor their kinetics of transport were affected (29). Nonetheless, the O-GlcNAc residues may have a more pronounced role in mammals, where OGT is essential.

We carried out O-GlcNAz-based crosslinking experiments to gain information about the direct binding partners of O-GlcNAc-modified FG-repeat nucleoporins. Notably, we obtained evidence for direct interactions between TNPO1 and both NUP153 and NUP358, a finding consistent with previous experiments (30–32). However, our cell-based crosslinking method enables additional conclusions. First, our data indicate that the observed interactions occur in a normal cellular environment, since the crosslinking event was triggered by irradiation of intact cells. Second, interactions occur at normal protein expression levels since our experiments involved crosslinking of endogenous proteins. Third, the formation of the covalent complex suggests the proteins interact directly, and not through a third party. Finally, because crosslinking occurs through the photoaffinity label on the GlcNAc, we conclude that there is an O-GlcNAc at or near the interaction site.

While our experiments do not directly address the question of whether the interactions between FG-repeat nucleoporins and nuclear transport factors are O-GlcNAc-dependent, these recognition events do share important features with typical glycan-mediated interactions. First, glycan-mediated interactions are typically low-affinity, with rapid off-rates (33). Similarly, interactions between FG-repeat nucleoporins and nuclear transport factors typically display nanomolar to micromolar equilibrium dissociation constants (34). Indeed, efficient nuclear transport requires that these interactions be transient, allowing cargo to be efficiently transported through the pore and not retained at a specific site. Second, both cell surface glycan-mediated interactions (35) and FG-repeat nucleoporin-nuclear transport factor interactions are typically multivalent (34, 36), which may enhance interaction specificity. Thus, the use of photocrosslinking groups offers an important strategy to covalently trap these transient and multivalent interactions (37).

In summary, we report a general method for identifying the interaction partners of O-GlcNAc-modified proteins and showed that this method can be applied in at least two cell lines. In the experiments presented here, we used antibodies against endogen-

ous proteins to isolate crosslinked complexes for further characterization. In the absence of suitable antibodies, epitope-tag could be appended to O-GlcNAcylated proteins to enable efficient analysis. We predict that this photocrosslinking approach could be applied to many of the other hundreds of proteins known to be O-GlcNAc-modified (5).

Methods

Synthesis of GlcNAz Compounds. Synthesis of Ac₄GlcNAz and UDP-GlcNAz have been described (16, 38). Ac₃GlcNAz-1-OH was produced by selective deprotection of Ac₄GlcNAzAc₃GlcNAz-1-P(Ac-SATE)₂ was synthesized by phosphorylation of Ac₃GlcNAz-1-OH with bis(5-acetyl-2-thioethyl) *N,N*-diisopropylphosphoramidite (20) and subsequent oxidation with mCPBA. *p*-nitrophenyl-β-D-GlcNAz (pNP-GlcNAz) was prepared by standard methods. Analytical data for Ac₃GlcNAz-1-P(Ac-SATE)₂ and pNP-GlcNAz are presented in Fig. S8.

HPAEC-PAD Analysis of GlcNAz-containing Metabolites. HeLa cells were transiently transfected with pCMV6-XL5-AGX1(F383G). After 43 h, cells were transferred to serum-free DMEM media containing low glucose (1.0 g/L). Ac₄GlcNAz, Ac₃GlcNAz-1-P(Ac-SATE)₂, Ac₄GlcNAc, or DMSO (vehicle) were added to achieve a final concentration of 100 μM. After 5 h, cells were harvested and lysed in 75% ethanol by sonication and centrifuged at 20,000 × *g*. Supernatant was dried, resuspended in 40 mM sodium phosphate buffer (20–60 μL per million cells), and filtered through Amicon® Ultra centrifugal filter unit (Millipore, 10,000 MWCO). Filtrates were analyzed by HPAEC (ICS-3000 system, Dionex) with CarboPac™MPA1 (Dionex) and pulsed amperometry detector (PAD) (39, 40).

Crosslinking of Cellular O-GlcNAz Proteins. HeLa cells were transiently transfected with mutant AGX1(F383G). Culture medium was replaced with serum-free, low-glucose DMEM 26 h after transfection. Ac₃GlcNAz-1-P(Ac-SATE)₂ (100 μM final concentration) was added at 26 h and/or 50 h after transfection. Cells were harvested 20 h after final addition of Ac₃GlcNAz-1-P(Ac-SATE)₂ and washed with DPBS. Cells were resuspended in DPBS and irradiated with UV light (365 nm, UVP, XX-20BLB lamp) while on an ice bath; control cells were kept on ice in dark. A 5% CuSO₄ pentahydrate aqueous solution was used to filter out longer wavelength light. Cells were lysed by RIPA buffer, and analyzed by SDS-PAGE and immunoblot.

Identification of Nucleoporin Interaction Partners. For immunoprecipitation of nucleoporins with mAb414, HeLa cells stably transfected with AGX1(F383G) were used. Ac₃GlcNAz-1-P(Ac-SATE)₂ (100 μM final concentration) was added 0 and 24 h after the medium was changed to serum-free, low-glucose (1.0 g/L) DMEM. Twenty h later, cells were harvested, UV irradiated, as described above, then lysed in an immunoprecipitation buffer (50 mM Tris-HCl, pH 8.0, 150 mM NaCl, 1.0% NP-40, 0.5% sodium deoxycholate, 2.0 mM EDTA, 1 mM DTT, 1 mM PMSF, 1 × protease inhibitor cocktail). After rotating the lysate with mAb414 (0.5 μL/mg lysate) overnight at 4 °C, the resulting solution was mixed with protein G sepharose (50 μL) for 4 h at 4 °C. After washing beads five times with the immunoprecipitation buffer, proteins were eluted with 50 μL of 2 × loading dye containing 5 mM DTT. Eluted samples were resolved by 5% SDS-PAGE, and silver staining was performed using the SilverQuest™ Silver staining kit (Invitrogen). Indicated regions of the gel were excised, destained, and in-gel digested with trypsin. Extracted peptides were analyzed by HPLC/MS/MS analysis.

ACKNOWLEDGMENTS. We thank Yuh Min Chook and Beatriz Fontoura for advice and discussions; Katharine Ullman, Mary Dasso, and Brian Burke for antinucleoporin antibodies; John Hanover, Suzanne Walker, and David Voadlo for plasmids; Junmei Zhang for mass spectrometry analysis; Masato Kato and Ilmin Kwon for recombinant OGT; and Shunzi (Susan) Li, Kathlynn Brown, and Tanya Leavy for peptide synthesis. This work was supported by a Welch Foundation grant (I-1686) to J.J.K., a National Institutes of Health grant (GM66047) to C.R.B., and a Howard Hughes Medical Institute fellowship of the Life Sciences Research Foundation to M.B. J.J.K. is an Alfred P. Sloan Research Fellow.

- Hart GW, Housley MP, Slawson C (2007) Cycling of O-linked β-N-acetylglucosamine on nucleocytoplasmic proteins. *Nature* 446:1017–1022.
- O'Donnell N, Zachara NE, Hart GW, Marth JD (2004) Ogt-dependent X-chromosome-linked protein glycosylation is a requisite modification in somatic cell function and embryo viability. *Mol Cell Biol* 24:1680–1690.
- Akimoto Y, Hart GW, Hirano H, Kawakami H (2005) O-GlcNAc modification of nucleocytoplasmic proteins and diabetes. *Med Mol Morphol* 38:84–91.

- Lazarus BD, Love DC, Hanover JA (2009) O-GlcNAc cycling: Implications for neurodegenerative disorders. *Int J Biochem Cell B* 41:2134–2146.
- Wang Z, Hart GW (2008) Glycomic approaches to study GlcNAcylation: Protein identification, site-mapping, and site-specific O-GlcNAc quantitation. *Clin Proteomics* 4:5–13.
- Love DC, Hanover JA (2005) The hexosamine signaling pathway: Deciphering the "O-GlcNAc Code". *Sci STKE* 2005:re13.

7. Hart GW, et al. (1995) O-linked N-acetylglucosamine: the "yin-yang" of Ser/Thr phosphorylation? Nuclear and cytoplasmic glycosylation. *Adv Exp Med Biol* 376:115–123.
8. Wang Z, Gucek M, Hart GW (2008) Cross-talk between GlcNAcylation and phosphorylation: Site-specific phosphorylation dynamics in response to globally elevated O-GlcNAc. *Proc Natl Acad Sci USA* 105:13793–13798.
9. Smet-Nocca C, et al. (2011) Identification of O-GlcNAc sites within peptides of the Tau protein and their impact on phosphorylation. *Mol Biosyst* 7:1420–1429.
10. Rexach JE, et al. (2010) Quantification of O-glycosylation stoichiometry and dynamics using resolvable mass tags. *Nat Chem Biol* 6:645–651.
11. Özcan S, Andrali SS, Cantrell JE (2010) Modulation of transcription factor function by O-GlcNAc modification. *Biochim Biophys Acta* 1799:353–364.
12. Gewinner C, et al. (2004) The coactivator of transcription CREB-binding protein interacts preferentially with the glycosylated form of Stat5. *J Biol Chem* 279:3563–3572.
13. Fujiki R, et al. (2009) GlcNAcylation of a histone methyltransferase in retinoic-acid-induced granulopoiesis. *Nature* 459:455–459.
14. Dentin R, Hedrick S, Xie J, Yates III J, Montminy M (2008) Hepatic glucose sensing via the CREB coactivator CRT2. *Science* 319:1402–1405.
15. Snow CM, Senior A, Gerace L (1987) Monoclonal antibodies identify a group of nuclear pore complex glycoproteins. *J Cell Biol* 104:1143–1156.
16. Bond MR, et al. (2011) Metabolism of diazirine-modified N-acetylmannosamine analogues to photo-cross-linking sialosides. *Bioconjug Chem* 22:1811–1823.
17. Kreppel LK, Hart GW (1999) Regulation of a cytosolic and nuclear O-GlcNAc transferase. *J Biol Chem* 274:32015–32022.
18. Leavy TM, Bertozzi CR (2007) A high-throughput assay for O-GlcNAc transferase detects primary sequence preferences in peptide substrates. *Bioorg Med Chem Lett* 17:3851–3854.
19. Bond MR, Whitman CM, Kohler JJ (2010) Metabolically incorporated photo-crosslinking sialic acid covalently captures a ganglioside-protein complex. *Mol Biosyst* 6:1796–1799.
20. Lefebvre I, et al. (1995) Mononucleoside phosphotriester derivatives with S-acyl-2-thioethyl bioreversible phosphate-protecting groups: Intracellular delivery of 3'-azido-2',3'-dideoxythymidine 5'-monophosphate. *J Med Chem* 38:3941–3950.
21. Peneff C, et al. (2001) Crystal structures of two human pyrophosphorylase isoforms in complexes with UDPGlc(Gal)NAc: role of the alternatively spliced insert in the enzyme oligomeric assembly and active site architecture. *EMBO J* 20:6191–6202.
22. Gross BJ, Kraybill BC, Walker S (2005) Discovery of O-GlcNAc transferase inhibitors. *J Am Chem Soc* 127:14588–14589.
23. Lazarus MB, Nam Y, Jiang J, Sliz P, Walker S (2011) Structure of human O-GlcNAc transferase and its complex with a peptide substrate. *Nature* 469:564–567.
24. Boyce M, et al. (2011) Metabolic cross-talk allows labeling of O-linked β -N-acetylglucosamine-modified proteins via the N-acetylgalactosamine salvage pathway. *Proc Natl Acad Sci USA* 108:3141–3146.
25. Zaro BW, Yang Y-Y, Hang HC, Pratt MR (2011) Chemical reporters for fluorescent detection and identification of O-GlcNAc-modified proteins reveal glycosylation of the ubiquitin ligase NEDD4-1. *Proc Natl Acad Sci USA* 108:8146–8151.
26. D'Angelo MA, Hetzer MW (2008) Structure, dynamics and function of nuclear pore complexes. *Trends Cell Biol* 18:456–466.
27. Chook YM, Süel KE (2011) Nuclear import by karyopherin- β s: Recognition and inhibition. *Biochim Biophys Acta* 1813:1593–1606.
28. Finlay DR, Newmeyer DD, Price TM, Forbes DJ (1987) Inhibition of in vitro nuclear transport by a lectin that binds to nuclear pores. *J Cell Biol* 104:189–200.
29. Hanover JA, et al. (2005) A *Caenorhabditis elegans* model of insulin resistance: Altered macronutrient storage and dauer formation in an OGT-1 knockout. *Proc Natl Acad Sci USA* 102:11266–11271.
30. Bonifaci N, Moroiaru J, Radu A, Blobel G (1997) Karyopherin β 2 mediates nuclear import of a mRNA binding protein. *Proc Natl Acad Sci USA* 94:5055–5060.
31. Hutten S, Wälde S, Spillner C, Hauber J, Kehlenbach RH (2009) The nuclear pore component Nup358 promotes transportin-dependent nuclear import. *J Cell Sci* 122:1100–1110.
32. Lau CK, et al. (2009) Transportin regulates major mitotic assembly events: From spindle to nuclear pore assembly. *Mol Biol Cell* 20:4043–4058.
33. Collins BE, Paulson JC (2004) Cell surface biology mediated by low affinity multivalent protein-glycan interactions. *Curr Opin Chem Biol* 8:617–625.
34. Terry LJ, Wenthe SR (2009) Flexible gates: Dynamic topologies and functions for FG nucleoporins in nucleocytoplasmic transport. *Euk Cell* 8:1814–1827.
35. Ramachandriaiah G, Chandra NR, Suroolia A, Vijayan M (2003) Computational analysis of multivalency in lectins: structures of garlic lectin-oligosaccharide complexes and their aggregates. *Glycobiology* 13:765–775.
36. Bednenko J, Cingolani G, Gerace L (2003) Importin β contains a COOH-terminal nucleoporin binding region important for nuclear transport. *J Cell Biol* 162:391–401.
37. Tanaka Y, Bond MR, Kohler JJ (2008) Photocrosslinkers illuminate interactions in living cells. *Mol Biosyst* 4:473–480.
38. Tanaka Y, Kohler JJ (2008) Photoactivatable crosslinking sugars for capturing glycoprotein interactions. *J Am Chem Soc* 130:3278–3279.
39. Tomiya N, Ailor E, Lawrence SM, Betenbaugh MJ, Lee YC (2001) Determination of nucleotides and sugar nucleotides involved in protein glycosylation by high-performance anion-exchange chromatography: Sugar nucleotide contents in cultured insect cells and mammalian cells. *Anal Biochem* 293:129–137.
40. Yu S-H, Bond MR, Whitman CM, Kohler JJ (2010) Metabolic labeling of glycoconjugates with photocrosslinking sugars. *Methods Enz* 478:541–562.

Supporting Information

Yu et al. 10.1073/pnas.1114356109

SI Text

SI Methods Materials for cell culture, immunoblotting, and immunoprecipitation. Dulbecco's Modified Eagle Medium (D-MEM) containing glucose (4.5 g/L or 1.0 g/L), L-glutamine, and 110 mg/L sodium pyruvate was purchased from Invitrogen. Fetal calf serum, penicillin/streptomycin, Dulbecco's Phosphate-Buffered Saline (DPBS), TrypLE™ Express Stable Trypsin-Like Enzyme with Phenol Red, Opti-MEM® I, and Lipofectamine™ 2000 were purchased from Invitrogen. The Invitrogen Countess Automated Cell Counter was used for cell counting. The bicinchoninic acid (BCA) Protein Assay Kit for determination of protein concentration was purchased from Pierce. For immunoblotting or immunoprecipitation, antibodies were obtained from the following sources: anti-biotin-HRP conjugate (Sigma-Aldrich), anti-O-GlcNAc (RL2, Thermo Fisher Scientific Inc., MA1-072), anti-O-GlcNAc (CTD110.6, Covance, MMS-248R), anti-SP1(PEP2) (Santa Cruz Biotechnology, SC-59), anti-TNPO1 [D45] (Abcam, ab10303), anti-NUP214 (Bethyl Lab, A300-716A), mAb414 (Covance Research Products), anti-NUP62 (BD Transduction Lab, 610497), anti-AGX1 (GeneTex, GTX103592). Anti-NUP358, a polyclonal anti-rabbit IgG was a generous gift from Mary Dasso (NIH) (1). Two anti-NUP153 were used. A polyclonal rabbit IgG against the zinc finger domain of human NUP153 was a generous gift from Katharine Ullman (University of Utah) (2) and was used for the experiments shown in Fig. 4, Fig. 5, and Fig. S5D. Anti-NUP153 (SA1) is a monoclonal mouse IgG against the C-terminal domain of NUP153. This was a generous gift from Brian Burke (Institute of Medical Biology, Singapore) and was used for the experiment shown in Fig. S4. Protein G Sepharose® (fast flow) was purchased from Sigma-Aldrich. Nitrocellulose membranes (Whatman Protran Rolls, BA79, 0.1 μ m) were purchased from Whatman. For chemiluminescent visualization, SuperSignal WestPico chemiluminescent substrate (ECL reagent) was purchased from Pierce. HeLa and T84 cells were obtained from the ATCC.

General materials and procedures for synthesis. Unless otherwise noted, chemicals were purchased from Sigma-Aldrich or Fisher Scientific. Analytical thin layer chromatography (TLC) was performed on silica gel 60 F254 glass plates (EM Science), staining the TLC was done by heating with ceric ammonium molybdate solution (CAM, 0.4% wt/v $\text{Ce}(\text{SO}_4)_2$, 10% wt/v ammonium molybdate tetrahydrate, and 10% sulfuric acid) or 5% phosphomolybdic acid in ethanol. Products were purified by flash column chromatography on silica gel 60 (particle size 40–63 or 60–200 μ m, EM Science). $^1\text{H-NMR}$, $^{13}\text{C-NMR}$, $^{31}\text{P-NMR}$ spectra were recorded with Varian 500 MHz spectrometers and reported in δ ppm scale. $^1\text{H-NMR}$ spectra were referenced to CDCl_3 (7.260 ppm). $^{13}\text{C-NMR}$ spectra were referenced to the center of the CDCl_3 triplet (77.0 ppm). Electrospray ionization mass spectrometry (ESI-MS) data were collected at the Protein Chemistry and Technology Center at UT Southwestern Medical Center. Samples were dissolved or diluted into either a solution that contained 50% acetonitrile and 5% NH_4OH or an acetonitrile: H_2O 1:1 solution that contained 0.1% formic acid. Proxeon nano-tips were used to infuse the samples into a QStar XL mass spectrometer (Applied Biosystems). Spectra were acquired with mass range m/z 50–1,000 or 300–1,000. Molecular weights were calculated using the Bayesian Protein Reconstruct tool of the Analyst QS1.1 software. High resolution ESI-TOF mass data were recorded on an Agilent ESI-TOF mass spectrometer at the Scripps Center for Mass Spectrometry, TSRI. Samples were electro-

sprayed into the TOF reflectron analyzer at an ESI voltage of 4000 V and a flow rate of 200 $\mu\text{L}/\text{min}$.

Synthesis of $\text{Ac}_3\text{GlcNDAz}$, $\text{Ac}_3\text{GlcNDAz-1-OH}$, $\text{Ac}_3\text{GlcNDAz-1-P}$, and UDP-GlcNDAz have been described elsewhere (3, 4). GlcNDAz-1-P as HPAEC standard was prepared by simple deacetylation of $\text{Ac}_3\text{GlcNDAz-1-P}$ with MeOH:Water:TEA (5:2:1) followed by cation exchange (Dowex 50WX8-100, H^+ form) and the resulting crude aqueous elute was used in HPAEC analysis without further purification. Synthesis of standard UDP-GalNDAz was essentially the same as that described for UDP-GlcNDAz (4, 5).

Synthesis of $\text{Ac}_3\text{GlcNDAz-1-P(Ac-SATE)}_2$. To the stirred solution of $\text{Ac}_3\text{GlcNDAz-1-OH}$ (100 mg, 0.241 mmol), and bis(*S*-acetyl-2-thioethyl) *N,N*-diisopropylphosphoramidite (0.336 mmol, 125 mg) in acetonitrile (700 μL) at 0°C , was added $^1\text{H-tetrazole}$ (0.361 mmol, 800 μL , 0.45 M in acetonitrile) and the resulting mixture was warmed to RT. After 1 h, mCPBA (0.361 mmol, 77%, 81.0 mg) was added at 0°C and stirred for additional 30 min at 0°C . The resulting reaction mixture was partitioned between ethyl acetate and 10% aqueous sodium sulfite (Na_2SO_3) and the organic layer was washed with saturated aqueous sodium bicarbonate (NaHCO_3) and brine. After two more extractions with fresh ethyl acetate from the aqueous phases, the combined organic layer was dried (Na_2SO_4) and concentrated by vacuum evaporation. The resulting residue was purified by flash silica gel column chromatography (ethyl acetate:hexanes = 1:1 and then ethyl acetate) to provide the $\text{Ac}_3\text{GlcNDAz-1-P(Ac-SATE)}_2$ as a colorless oil (145 mg, 86%). $^1\text{H NMR}$ (500 MHz, CDCl_3): δ 1.00 (s, 3H, $\text{NHCOCH}_2\text{CH}_2(\text{N}=\text{N})\text{CH}_3$), 1.68–1.79 (m, 2H, $\text{NHCOCH}_2\text{CH}_2(\text{N}=\text{N})\text{CH}_3$), 1.90–2.00 (m, 2H, $\text{NHCOCH}_2\text{CH}_2(\text{N}=\text{N})\text{CH}_3$), 2.02 (s, 6H, O-COCH₃), 2.16 (s, 3H, O-COCH₃), 2.36–2.39 (2s, 6H, S-COCH₃), 3.18 (m, 4H, -OCH₂CH₂Sac), 4.05–4.29 (m, 7H, -OCH₂CH₂Sac \times 2, H₅, H_{6a}, H_{6b}), 4.47(m, 1H, H₂), 5.21(m, 2H, H₃ & H₄), 5.56 (dd, $J = 5.6, 3.3$ Hz, 1H, H₁), 6.31 (d, $J = 9.0$ Hz, 1H, NH). $^{13}\text{C NMR}$ (125 MHz, CDCl_3): δ 19.8, 20.5, 20.6, 25.4, 29.0(m), 29.5, 30.1, 30.5 (m), 51.5(d), 61.3, 66.4(m), 67.4, 69.6, 96.3(d), 169.1, 170.5, 171.0, 171.7, 194.7, 195.1. $^{31}\text{P NMR}$ (200 MHz, CDCl_3): δ -2.28. ESI-MS: calcd. for $\text{C}_{25}\text{H}_{39}\text{N}_3\text{O}_{14}\text{PS}_2$ [$\text{M} + \text{H}$]⁺ 700.16, found 700.14; calcd. for $\text{C}_{25}\text{H}_{38}\text{N}_3\text{NaO}_{14}\text{PS}_2$ [$\text{M} + \text{Na}$]⁺ 722.14, found 722.13. HRMS (ESI-TOF) calcd. for $\text{C}_{25}\text{H}_{39}\text{N}_3\text{O}_{14}\text{PS}_2$ [$\text{M} + \text{H}$]⁺ 700.1605, found 700.1607; calcd. for $\text{C}_{25}\text{H}_{38}\text{N}_3\text{NaO}_{14}\text{PS}_2$ [$\text{M} + \text{Na}$]⁺ 722.1425, found 722.1421. NMR spectra are shown in Fig. S8 A–C.

Synthesis of *p*-nitrophenyl- β -D-GlcNDAz (pNP-GlcNDAz). pNP-GlcNDAz was synthesized by adapting reported protocols for related molecules (6, 7). GlcNDAz (105 mg, 0.363 mmol) was suspended in acetyl chloride (900 μL) at 0°C and the resulting mixture was warmed to RT. After 16 h, the mixture was diluted with chloroform and poured onto ice in a separatory funnel. Saturated aqueous sodium bicarbonate (NaHCO_3) was added to quench the remaining acetyl chloride. After partitioning, the organic layer was washed with brine, dried (Na_2SO_4), and then concentrated by vacuum evaporation. After resuspending the dried crude mixture in dichloromethane (2 mL), tetrabutylammonium hydrogen sulfate (0.363 mmol, 123 mg), 4-nitrophenol (0.726 mmol, 101 mg), and then 1N NaOH (2 mL) were added. After vigorous stirring for 3 h, the reaction mixture was diluted with ethyl acetate (20 mL) and washed with 1 M NaOH (10 mL, five times), water (10 mL, three times), and brine. The

ethyl acetate layer was dried with Na_2SO_4 and concentrated by vacuum evaporation. The resulting concentrate was precipitated by ethyl acetate and hexane (1:2–1:3) and the precipitate was collected by filtration. The resulting precipitate was recrystallized in ethyl acetate and hexane (1:3) overnight to give 4-nitrophenyl-3,4,6-tri-O-acetyl- β -D-GlcNDaz (60.6 mg, 0.113 mmol, 31.1% over two steps). ^1H NMR (500 MHz, CDCl_3): δ 0.96 (s, 3H, $\text{NHCOCH}_2\text{CH}_2(\text{N}=\text{N})\text{CH}_3$), 1.69–1.79 (m, 2H, $\text{NHCOCH}_2\text{CH}_2(\text{N}=\text{N})\text{CH}_3$), 1.84–1.94 (m, 2H, $\text{NHCOCH}_2\text{CH}_2(\text{N}=\text{N})\text{CH}_3$), 2.06 (s, 3H, O-COCH₃), 2.08 (s, 3H, O-COCH₃), 3.96 (m, 1H, H₅) 4.09–4.18 (m, 2H, H₂, H_{6a}), 4.28 (dd, $J = 12.3, 5.6$ Hz, 1H, H_{6b}), 5.13 (t, $J = 9.6$ Hz, 1H, H₃ or H₄), 5.41–5.49 (m, 2H, H₁ and H₄ or H₃), 5.80 (d, $J = 8.4$ Hz, 1H, NH), 7.06 (d, $J = 9.1$ Hz, 2H, phenyl), 8.16 (d, $J = 9.1$ Hz, 2H, phenyl). ^{13}C NMR (125 MHz, CDCl_3): δ 19.8, 20.6, 20.7, 25.3, 29.1, 30.4, 54.7, 62.0, 68.3, 71.4, 72.2, 97.7, 116.5, 125.7, 142.9, 161.4, 169.4, 170.4, 170.8, 171.7. MALDI-TOF-MS: calcd. for $\text{C}_{23}\text{H}_{28}\text{N}_4\text{NaO}_{11}$ [$\text{M} + \text{Na}$]⁺, 599.16, found 599.20; calcd. for $\text{C}_{23}\text{H}_{28}\text{N}_2\text{NaO}_{11}$ [$\text{M} + \text{Na} - \text{N}_2$]⁺, 531.16, found 531.20; calcd. for $\text{C}_{23}\text{H}_{29}\text{N}_2\text{O}_{11}$ [$\text{M} + \text{H} - \text{N}_2$]⁺, 509.18, found 509.22.

To the solution of 4-nitrophenyl-3,4,6-tri-O-acetyl-GlcNDaz (46 mg, 0.086 mmol) in methanol (2.5 mL), was added NaOMe (0.1 eq., 8.6 μmol , 0.5 M in MeOH, 17 μL) and the resulting mixture was stirred for 2 h at RT. After filtration, the precipitate was washed with cold methanol to give pure pNP-GlcNDaz (12.7 mg) and the filtrate was passed through Dowex® 50WX8-100, H^+ form and then concentrated to obtain 22.8 mg of pNP-GlcNDaz (quantitative yield). ^1H NMR (500 MHz, CD_3OD): δ 0.97 (s, 3H, $\text{NHCOCH}_2\text{CH}_2(\text{N}=\text{N})\text{CH}_3$), 1.65 (t, $J = 7.7$ Hz, 2H, $\text{NHCOCH}_2\text{CH}_2(\text{N}=\text{N})\text{CH}_3$), 2.06–2.18 (m, 2H, $\text{NHCOCH}_2\text{CH}_2(\text{N}=\text{N})\text{CH}_3$), 3.43 (t, $J = 9.5$ Hz, 1H, H₃ or H₄), 3.50 (m, 1H, H₅), 3.60 (dd, $J = 10.2, 8.9$ Hz, H₄ or H₃), 3.72 (dd, $J = 12.15, 5.8$ Hz, 1H, H_{6a}), 3.91–3.97 (m, 2H, H₂ & H_{6b}), 5.21 (d, $J = 8.4$ Hz, 1H, H₁), 7.18 (d, $J = 9.2$ Hz, 2H, phenyl), 8.20 (d, $J = 9.2$ Hz, 2H, phenyl). ^{13}C NMR (125 MHz, CD_3OD): δ 19.7, 26.4, 31.4, 31.6, 57.0, 62.4, 71.7, 75.6, 78.5, 99.9, 117.6, 126.6, 143.9, 163.7, 175.1. HRMS (ESI-TOF): calcd. for $\text{C}_{17}\text{H}_{23}\text{N}_4\text{O}_8$ [$\text{M} + \text{H}$]⁺, 411.1516, found 411.1513; calcd. for $\text{C}_{17}\text{H}_{22}\text{N}_4\text{NaO}_8$ [$\text{M} + \text{Na}$]⁺, 433.1335, found 433.1330. Stereochemistry of the anomeric position was determined based on the coupling constant of H₁(d, $J = 8.4$ Hz). NMR spectra are shown in Fig. S8 D and E.

Synthesis of peptide substrates. Biotinylated CKII peptide [NH_2 -PGGSTPVSSANMMK(biotin)-COOH] was synthesized essentially as described for other peptides (8). A modified human α -A crystallin peptide termed +P2 (Ac-AIPVSRPEK-CONH₂) was synthesized by standard peptide synthesis methods.

Evaluation of human OGT activity with UDP-GlcNDaz. For the lysate experiment (Fig. S1B), HeLa cells were transiently transfected with 24 μg of pCDNA4/TO/ncOGT-myc-His (9) using Lipofectamine® 2000. After 48 h, cells (approximately 10×10^6) were harvested and lysed in a transferase assay buffer [400 μL , 25 mM Hepes, 10 mM MgCl_2 , 1 mM EDTA, 1 mM PMSF, and 1 \times protease inhibitor cocktail (Complete Mini, Roche)] via sonication (five times for 5 s each, VirSonic 100, VirTis) on ice. After centrifugation ($20,000 \times g$, 10 min), the supernatant was collected and mixed with 800 μL of 30% PEG8000 (in 25 mM Hepes, 10 mM MgCl_2 , 1 mM EDTA) and the mixture was vortexed briefly and centrifuged ($20,000 \times g$, 20 min, 4°C). After removing the supernatant, the resulting protein pellet was resuspended in 200 μL of transferase assay buffer (25 mM Hepes, 10 mM MgCl_2 , 1 mM EDTA). After determination of the protein concentration by the bicinchoninic acid assay (BCA), the transferase assay was performed by reaction of 100 μg of the lysate, 100 μM of synthetic +P2 peptide, and UDP-sugar [0.5 mM UDP-GlcNAc,

0.5 mM UDP-GlcNDaz, or 1:1 mixture of UDP-GlcNAc and UDP-GlcNDaz (each 0.5 mM)] in 25 mM Hepes, 10 mM MgCl_2 , 1 mM EDTA for 16 h at RT. After the reaction, the peptide was purified by Zip-Tip_{C18} (Millipore) and analyzed by MALDI-TOF MS using a matrix of DHB containing aniline in 50% acetonitrile.

For the competition experiment with recombinant ncOGT (Fig. S1C), ncOGT expression and purification were performed using a codon-optimized plasmid generously supplied by Suzanne Walker (Harvard Medical School), following the previously reported method (10). Reaction mixtures contained 2 μM recombinant ncOGT, 100 μM +P2 peptide, UDP-sugar (2 mM UDP-GlcNAc, 2 mM UDP-GlcNDaz, or 2 mM of each) in 20 mM Tris-HCl buffer pH 7.5, containing 12.5 mM MgCl_2 and 2 mM β -mercaptoethanol. Reaction mixtures were incubated at 37°C for 15 h, then filtered using an Amicon® Ultra centrifugal filter unit (Millipore, 10,000 MWCO). Filtrates were analyzed by HPLC by injecting 100 μL of each onto a ZORBAX Eclipse XDB-phenyl column (4.6 \times 150 mm, particle size 3.5 μm) attached to a Dynamax SD-200 HPLC system. The eluents used were 0.1% TFA in water (E1) and 0.1% TFA in acetonitrile (E2). HPLC was performed with a flow rate of 1.5 mL/min and following gradient elution was used: T (0 min) = 5% E2, T (3 min) = 5% E2, T (5 min) = 10% E2, T (20 min) = 20% E2, T (22 min) = 100% E2, T (25 min) = 100% E2, T (28 min) = 5% E2, T (30 min) = 5% E2. Chromatograms were recorded with UV detector (Dynamax UV-C) set at 220 nm. Molar absorption coefficients (220 nm) for the O-GlcNAc-modified and O-GlcNDaz-modified peptides were estimated, based on the measured absorbance values for the unmodified peptide, GlcNAc, and GlcNDaz. Identities of the peaks corresponding to the +P2 peptide, the O-GlcNAc-modified peptide, and the O-GlcNDaz-modified peptide were confirmed by MALDI-TOF analysis of the collected fractions. The peak assigned as the O-GlcNDaz-modified peptide was also shown to be sensitive to UV irradiation.

Crosslinking O-GlcNDaz peptide with anti-O-GlcNAc antibodies. For the in vitro transfer and crosslinking experiments (Figs. S1A and S2), the plasmid used for recombinant ncOGT expression was a generous gift from John Hanover (NIDDK) (11). ncOGT expression and purification were performed as described previously (8, 12). In vitro OGT reactions with synthetic biotin-CK2 peptide (100 μM) were performed in 20 mM Tris-HCl pH 7.2, 12.5 μM MgCl_2 , 715 μM β -mercaptoethanol and 100 μM of UDP-GlcNAc, UDP-GlcNDaz, or water at 37°C for 16 h. Peptides were purified via Zip-Tip_{C18} (Millipore) and analyzed by MALDI-TOF (Fig. S1A). Peptide samples were incubated overnight at 4°C with RL2 or CTD110.6. Each sample was split in half, with one half receiving 20 min of UV irradiation (365 nm, XX-20BLB, UVP, 40 min). Samples were resolved on SDS-PAGE gels in duplicate and transferred to nitrocellulose. The blots were probed with an anti-biotin-HRP antibody (1:50,000)(Fig. S2B).

Mutagenesis of AGX1. Human AGX1 gene in pCMV6-XL5-UAP1 (Origene) was used as a template for constructing mutants pCMV6-XL5-AGX1(F381G) and pCMV6-XL5-AGX1(F383G) by QuikChange mutagenesis protocol (Stratagene) using the following primer sets:

AGX1(F381G) forward: CCC AAT GGA ATA AAG ATG GAA AAA GGT GTC TTT GAC ATC TTC CAG

AGX1(F381G) reverse: CTG GAA GAT GTC AAA GAC ACC TTT TTC CAT CTT TAT TCC ATT GGG

AGX1(F383G) forward: CCC ATT GGA ATA AAG ATG GAA AAA TTT GTC GGT GAC ATC TTC CAG

AGX1(F383G) reverse: CTG GAA GAT GTC ACC GAC AAA TTT TTC CAT CTT TAT TCC ATT GGG

Mutant plasmids were sequenced by the DNA sequencing core facility in McDermott Center for Human Growth & Development (University of Southwestern Medical Center).

Stable expression of AGX1(F383G) in HeLa cells. The gene encoding AGX1(F383G) was amplified from pCMV6-XL5-AGX1(F383G) by PCR using the following primers:

5'-BamHI-primer: ATAGGATCCATGAACATTAATGAC-CTCAAACCT

3'-NotI-primer: TATGCGGCCGCTCAAATACCATTTTT-CACCACT

The PCR product and pIRESpuo3 vector were each digested with BamHI and NotI, then ligated together. The identity of the desired plasmid (pIRESpuo3-AGX1(F383G)) was confirmed by DNA sequencing.

HeLa cells were transfected with pIRESpuo3-AGX1(F383G) using Lipofectamine-2000. After 48 h, puromycin (5 $\mu\text{g}/\text{mL}$) was added. Medium containing puromycin was replaced every two or three days. After 24 d of selection, surviving cells were maintained in DMEM containing 1 $\mu\text{g}/\text{mL}$ puromycin. Those stably transfected cells were cultured with $\text{Ac}_3\text{GlcNDAz-1-P}(\text{Ac-SATE})_2$. HPAEC analysis of the lysates revealed UDP-GlcNDAz production, confirming stable expression of AGX1(F383G). Overexpression of AGX1 was also determined by immunoblotting (Fig. S6A); assignment of bands corresponding to AGX1 and AGX2 was based on literature precedent (13).

HPAEC-PAD analysis of lysates. Lysates were prepared as described in the main text. The eluents used were 1.0 mM NaOH (E1) and 1.0 M NaOAc and 1.0 mM NaOH (E2). HPAEC was performed with a flow rate = 1 mL/min and the following gradient elution was performed: $T_{0 \text{ min}} = 5\% \text{ E2}$, $T_{40} = 30\% \text{ E2}$, $T_{45} = 50\% \text{ E2}$, $T_{60} = 55\% \text{ E2}$, $T_{65} = 100\% \text{ E2}$, $T_{75} = 100\% \text{ E2}$, $T_{80} = 5\% \text{ E2}$, $T_{90} = 5\% \text{ E2}$. GlcNDAz-1-P eluted at 20.8 min and its identity was confirmed by parallel injection of standard GlcNDAz-1-P (Fig. S3A). UDP-GlcNDAz eluted at 62.5 min and its identity was confirmed by parallel injection of standard UDP-GlcNDAz (Fig. S3B). Also, the lysate was irradiated by UV (365 nm, XX-20BLB, UVP, 45 min) and its HPAEC chromatogram was compared with that of UV-irradiated GlcNDAz-1-P standard compound or UV-irradiated UDP-GlcNDAz standard compound (Fig. S3A and B). The peak eluting at 62.5 min from the HeLa lysate was collected, desalted by cation-exchange resin (Dowex® 50WX8-100, ammonium form) and then lyophilized for the MALDI-TOF mass analysis (Fig. S3C), which also confirmed the production of UDP-GlcNDAz in HeLa cells.

Crosslinking lysates with anti-O-GlcNAc antibody. HeLa cells were transiently transfected with 24 μg of pCMV6-XL5-AGX1(F383G), 24 μg of pCDNA4/TO/ncOGT-myc-His, or 12 μg each of pCMV6-XL5-AGX1(F383G) and pCDNA4/TO/ncOGT-myc-His using Lipofectamine-2000. After 48 h, 20 μL of 50 mM $\text{Ac}_3\text{GlcNDAz-1-P}(\text{Ac-SATE})_2$ in DMSO or DMSO alone was added to the cells in serum-free, low-glucose (1.0 g/L) DMEM. After 19 h, cells were harvested and lysed with RIPA buffer (50 mM Tris-HCl pH 8.0, 150 mM NaCl, 1.0% NP-40, 0.5% sodium deoxycholate, 0.1% SDS, 1 mM PMSF, 1 \times protease inhibitor cocktail) via vortexing (20 sec) followed by incubation in ice (30 min). Lysates were centrifuged (20,000 $\times g$, 10 min). The supernatant was collected and the buffer was exchanged with fresh RIPA buffer by Zeba™ spin desalting columns (MWCO = 7,000, Pierce) following the manufacturer's protocol. After supplementing the desalted lysate with PMSF and protease inhibitor cocktail, the protein concentration was determined by the BCA method. Each 1.3 mg of lysate was rotated with RL2 (Affinity Bio Reagent, 2.6 μg) in 650 μL total volume at 4°C. After overnight rotation, one half of each lysate was irradiated by UV (365 nm,

XX-20BLB, UVP, 40 min) in 24-well dish on ice bath, while the other half was kept on ice in dark. Each sample was collected and rotated with protein G Sepharose (20 μL each, Sigma-Aldrich) at 4°C and the beads were washed three times with the RIPA buffer. Proteins were eluted from the washed beads with 2 \times loading dye by heating at 95°C for 7 min. The eluted samples were resolved by SDS-PAGE and then transferred to nitrocellulose membrane (17 h, 30 V) at 4°C. Immunoblotting was performed using anti-SP1 antibody (Santa Cruz) or mouse anti-NUP153 antibody (SA-1 from Brian Burke) (Fig. S4). This experiment demonstrated that cotransfection with pCDNA4/TO/ncOGT-myc-His had no effect on crosslinking efficiency, so pCDNA4/TO/ncOGT-myc-His was not included in any other experiments.

Experiments in AGX1(F383G)-expressing T84 cells. To demonstrate that crosslinking could be performed in other cell types (Fig. S5 C and D), T84 cells stably expressing AGX1(F383G) were used. T84 cells stably expressing mutant AGX1(F383G) were prepared by lentiviral transduction as follows. Site-directed mutagenesis was performed on the vector pCMV6-XL5-AGX1(F383G) to destroy an intrinsic EcoRI site located within the AGX1 gene, and the AGX1(F383G) PCR product obtained from that plasmid was then cloned into the SpeI and EcoRI restriction sites of the linearized pSIN4-EF2-IRES-Puro lentiviral vector (a kind gift from Dr. Jiang Wu at UT Southwestern) (14). The pSIN4-EF2-AGX1(F383G)-IRES-Puro vector was utilized to assemble lentivirus with a 2nd-generation packaging system following the protocol published by the RNAi Consortium (http://www.broad.mit.edu/genome_bio/trc/rnai.html). The lentiviral packaging plasmid psPAX2 (Addgene plasmid 12260) and envelope plasmid pMD2.G (Addgene plasmid 12259) were obtained from Dr. Didier Trono. T84 cells were infected for 20 h in D-MEM/F-12 (1:1)-Hepes media (containing glucose (3.151 g/L), L-glutamine, 5% FBS, and penicillin/streptomycin) with 8 $\mu\text{g}/\text{mL}$ of Polybrene (Sigma-Aldrich). Cells were infected with a targeted MOI $\ll 1$ such that each cell is only likely to be infected once. Stably transduced T84 cells were subjected to selection with 7 $\mu\text{g}/\text{mL}$ puromycin for 17 d before the puromycin selection was removed. For the crosslinking experiments, the T84 cells stably expressing mutant AGX1 were cultured with $\text{Ac}_3\text{GlcNDAz-1-P}(\text{Ac-SATE})_2$ (100 μM final concentration) or DMSO (vehicle) added at 0 h and at 24 h after the media was changed to serum-free D-MEM/F-12 (1:1)-Hepes. Cells were harvested 20 h after the second addition of $\text{Ac}_3\text{GlcNDAz-1-P}(\text{Ac-SATE})_2$ and UV irradiated, as described in the main text. The UV-irradiated cells were lysed as described above and the lysate was resolved by SDS-PAGE and transferred to nitrocellulose membrane (17 h, 30 V) at 4°C. Immunoblotting was performed using mAb414 or rabbit anti-NUP153 antibody (from Katharine Ullman).

In-gel digestion of silver-stained proteins. Regions of interest were excised from the silver-stained gel. The gel slices were washed three times with an acidic buffer [acetic acid:ethanol:water = 10:50:40, (v/v/v)] for 24 h. After being swollen in water twice (15 min each time), the gel bands were treated with a destaining solution containing 15 mM potassium ferricyanide and 50 mM sodium thiosulfate. After extensive washing, the gel bands were cut into small pieces, dehydrated in acetonitrile, and then dried in a SpeedVac (Thermo Electron). A sufficient amount of trypsin (10 ng/ μL in 50 mM ammonium bicarbonate) was added to cover the gel pieces and overnight digestion was performed at 37°C. The resulting tryptic peptides were extracted sequentially with 5% TFA/50% acetonitrile/45% water (v/v/v), 0.1% TFA/75% acetonitrile/24.9% water (v/v/v), and 100% acetonitrile. The extracts were combined and dried in a SpeedVac. Desalting was achieved with C18 ZipTips (Millipore) according to the manufacturer's instructions, prior to nano-HPLC/mass spectrometric analysis.

Identification of proteins by HPLC/MS/MS analysis. Mass spectrometry was performed at the UT Southwestern Protein Chemistry Technology Center. High performance liquid chromatography tandem mass spectrometry (HPLC/MS/MS) analysis was performed on an integrated system that includes an Agilent 1100 series nanoflow LC system (Agilent) and a LTQ 2D trap mass spectrometer (Thermo Electron) equipped with a nano-electrospray ionization (NSI) source. Tryptic peptides were reconstituted in buffer A solution (0.05% formic acid, 2% acetonitrile, 97.95% H₂O, v/v/v), and separated by a capillary HPLC column (11 cm length × 75 μm I.D.) packed in-house with Luna C18 resin (5 μm particle size, 100 Å pore diameter, Phenomenex). A 40 min gradient from 20% to 90% buffer B (0.05% formic acid, 90% acetonitrile, 9.95% H₂O, v/v/v) was used. The eluted peptides were electrosprayed directly into the LTQ ion trap mass spectrometer, which was operated in a data-dependent mode. Mascot (version 2.2, Matrix Science) was used for database search.

NCOAT specificity assay. Artificial O-GlcNAc and O-GlcNAz substrates were used for this chromogenic assay (15, 16).

- Joseph J, Liu S-T, Jablonski SA, Yen TJ, Dasso M (2004) The RanGAP1-RanBP2 complex is essential for microtubule-kinetochore interactions *in vivo*. *Curr Biol* 14:611–617.
- Liu J, Prunuske AJ, Fager AM, Ullman KS (2003) The COPI complex functions in nuclear envelope breakdown and is recruited by the nucleoporin Nup153. *Dev Cell* 5:487–498.
- Tanaka Y & Kohler JJ (2008) Photoactivatable crosslinking sugars for capturing glyco-protein interactions. *J Am Chem Soc* 130:3278–3279.
- Bond MR, et al. (2011) Metabolism of diazirine-modified *N*-acetylmannosamine analogues to photo-cross-linking sialosides. *Bioconjug Chem* 22:1811–1823.
- Bond MR (2010) Illuminating glycoconjugate interactions and glycosyltransferase substrates using photocrosslinking sugar analogs. Ph.D. (Stanford University, Stanford, CA).
- Vocadlo DJ, Withers SG (2005) Detailed comparative analysis of the catalytic mechanisms of β-*N*-acetylglucosaminidases from families 3 and 20 of glycoside hydrolases. *Biochemistry* 44:12809–12818.
- Orth R, Pitscheider M, Sieber SA (2010) Chemical probes for labeling of the bacterial glucosaminidase NagZ via the Huisgen cycloaddition. *Synthesis* 2010:2201–2206.
- Leavy TM, Bertozzi CR (2007) A high-throughput assay for O-GlcNAc transferase detects primary sequence preferences in peptide substrates. *Bioorg Med Chem Lett* 17:3851–3854.
- Boyce M, et al. (2011) Metabolic cross-talk allows labeling of O-linked β-*N*-acetylglucosamine-modified proteins via the *N*-acetylgalactosamine salvage pathway. *Proc Natl Acad Sci USA* 108:3141–3146.
- Gross BJ, Kraybill BC, Walker S (2005) Discovery of O-GlcNAc transferase inhibitors. *J Am Chem Soc* 127:14588–14589.
- Lubas WA, Frank DW, Krause M, Hanover JA (1997) O-linked GlcNAc transferase is a conserved nucleocytoplasmic protein containing tetratricopeptide repeats. *J Biol Chem* 272:9316–9324.
- Vocadlo DJ, Hang HC, Kim EJ, Hanover JA, Bertozzi CR (2003) A chemical approach for identifying O-GlcNAc-modified proteins in cells. *Proc Natl Acad Sci USA* 100:9116–9121.
- Wang-Gillam A, Pastuszak I, Elbein AD (1998) A 17-amino acid insert changes UDP-*N*-acetylhexosamine pyrophosphorylase specificity from UDP-GalNAc to UDP-GlcNAc. *J Biol Chem* 273:27055–27057.
- Zhan X, Shi X, Zhang Z, Chen Y, Wu JI (2011) Dual role of Brg chromatin remodeling factor in Sonic hedgehog signaling during neural development. *Proc Natl Acad Sci USA* 108:12758–12763.
- Gao Y, Wells L, Comer FI, Parker GJ, Hart GW (2001) Dynamic O-glycosylation of nuclear and cytosolic proteins. *J Biol Chem* 276:9838–9845.
- Kang HT, Ju JW, Cho JW, Hwang ES (2003) Down-regulation of Sp1 activity through modulation of O-glycosylation by treatment with a low glucose mimetic, 2-deoxyglucose. *J Biol Chem* 278:51223–51231.

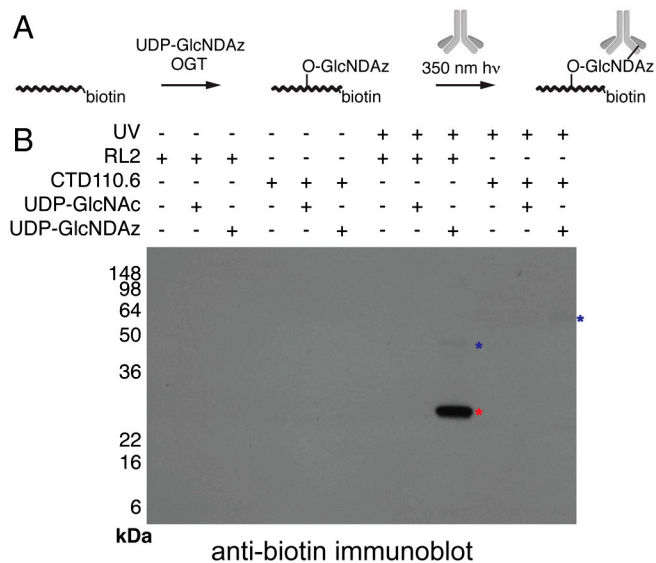


Fig. S2. Covalent crosslinking of an O-GlcNAc-mediated interaction using diazirine-modified O-GlcNAc (O-GlcNDAz). (A) Recombinant human ncOGT was incubated with UDP-GlcNDAz and a biotinylated CKII peptide [PGGSTPVSSANMMK(biotin)]. The partially purified peptide was incubated with an O-GlcNAc-recognizing antibody (either RL2 or CTD110.6) and irradiated with 365 nm light. (B) Antibiotin immunoblotting revealed a biotinylated species whose molecular weight is consistent with a covalent adduct formed from the CK2 peptide and the light chain of RL2 (red asterisk). Formation of the biotinylated product was dependent on the inclusion of UDP-GlcNDAz and administration of UV irradiation. Weaker bands corresponding to peptide crosslinking to the heavy chains of RL2 and CTD110.6 were also observed (blue asterisks). While we observe strong crosslinking of biotinylated peptide to the light chain of RL2, crosslinking to CTD110.6 was barely detectable. The reasons behind the lack of crosslinking to the CTD110.6 antibody are unclear: CTD110.6 may not recognize the CKII peptide well, the addition of crosslinker may interfere with recognition, or the orientation of the crosslinker may be poorly suited for crosslinking. We did not perform additional experiments to distinguish among these possibilities.

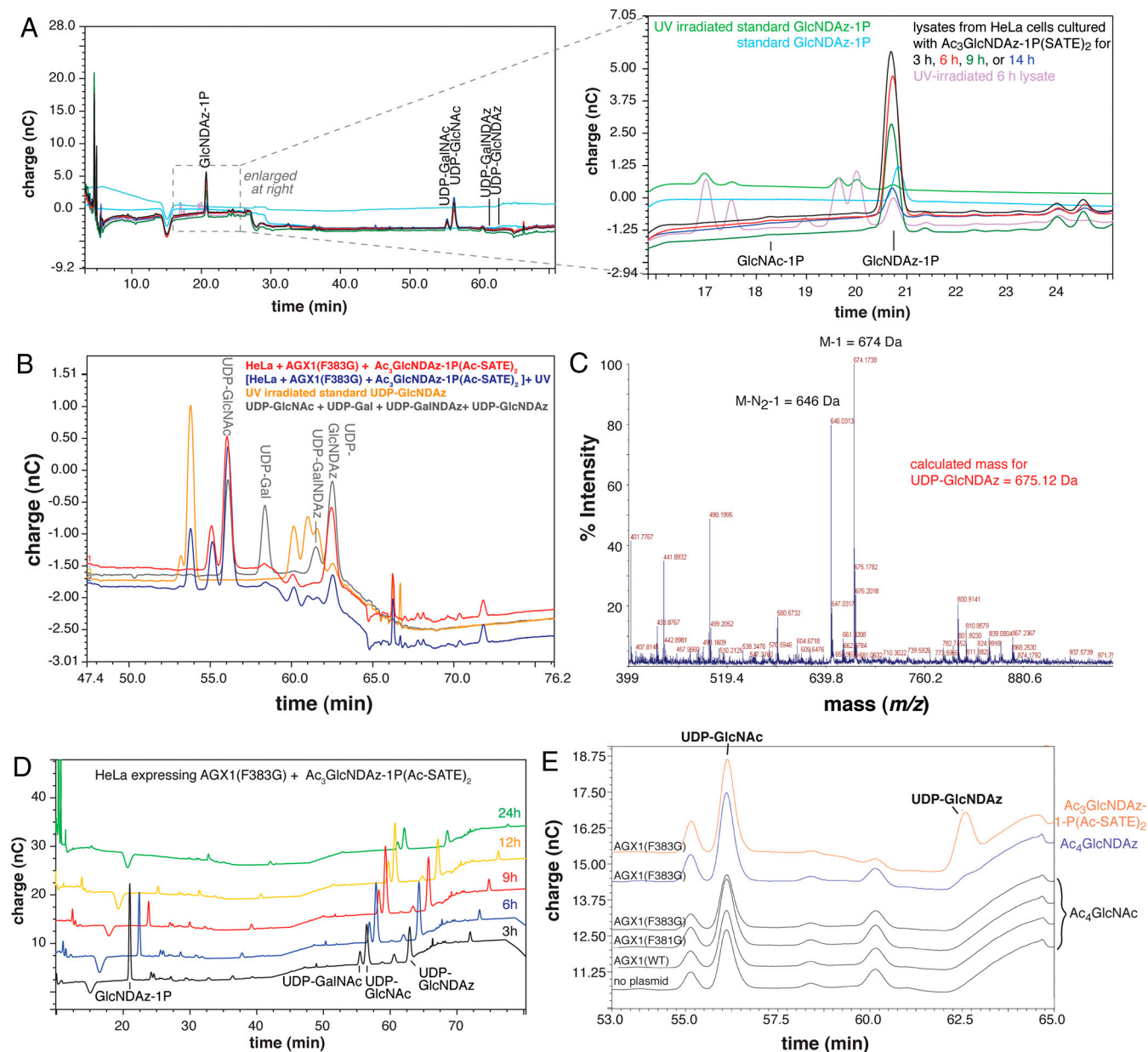


Fig. S3. Metabolism of $\text{Ac}_3\text{GlcNDAz-1-P(Ac-SATE)}_2$ to UDP-GlcNDAz. (A) HeLa cells were cultured with $\text{Ac}_3\text{GlcNDAz-1-P(Ac-SATE)}_2$ for 3, 6, 9, or 14 h, then lysed. Cell lysates were analyzed by HPAEC-PAD. Both the full chromatogram and the GlcNDAz-1-P region are shown. A peak with the same retention time as standard GlcNDAz-1-P was observed rapidly (as early as 3 h) and decreased over time. UV irradiation of both the lysate and GlcNDAz-1-P standard resulted in loss of the GlcNDAz-1-P peak and production of characteristic new peaks. Production of UDP-GlcNDAz was not observed. (B) HeLa cells were transiently transfected with pCMV6-XL5-AGX1(F383G) and cultured with $\text{Ac}_3\text{GlcNDAz-1-P(Ac-SATE)}_2$. HPAEC-PAD analysis of the cell lysates revealed new peak whose retention time matched that of synthetic UDP-GlcNDAz. In addition, UV irradiation of the lysate resulted in decreased intensity of the putative UDP-GlcNDAz peak, along with the production of new peaks. The new peaks were similar to those observed upon irradiation of the standard UDP-GlcNDAz molecule. (C) The lysate peak eluting at 62.5 min (B) was collected and analyzed by MALDI-TOF mass spectrometry (anionic and reflector mode), revealing a mass (m/z) consistent with the value predicted for UDP-GlcNDAz. (D) HeLa cells were transiently transfected with pCMV6-XL5-AGX1(F383G) and cultured with $\text{Ac}_3\text{GlcNDAz-1-P(Ac-SATE)}_2$ for 3, 6, 9, 12, or 24 h. Lysates were analyzed by HPAEC-PAD. GlcNDAz-1-P levels decreased over the time frame examined, while UDP-GlcNDAz levels increased and then decreased. (E) HeLa cells were transiently transfected with pCMV6-XL5-AGX1(WT), pCMV6-XL5-AGX1(F381G), or pCMV6-XL5-AGX1(F383G) or no plasmid and cultured with Ac_4GlcNAc , $\text{Ac}_4\text{GlcNDAz}$, or $\text{Ac}_3\text{GlcNDAz-1-P(Ac-SATE)}_2$, as indicated. Only cells cultured with $\text{Ac}_3\text{GlcNDAz-1-P(Ac-SATE)}_2$ demonstrated efficient UDP-GlcNDAz production, indicated that $\text{Ac}_4\text{GlcNDAz}$ is not efficiently metabolized to GlcNDAz-1-P in these cells.

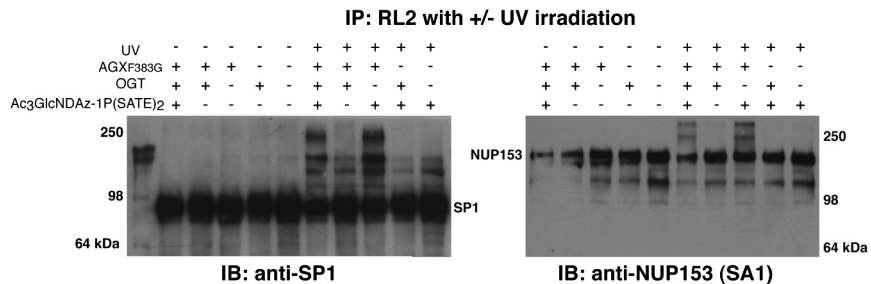


Fig. S4. Crosslinking of O-GlcNDAz-ylated proteins in lysates. HeLa cells were transiently transfected with pCMV6-XL5-AGX1(F383G) and/or pCDNA4/TO/ncOGT-myc-His. Cells were cultured with Ac₃GlcNDAz-1-P(Ac-SATE)₂. Cells were lysed and the lysates were incubated with RL2 (anti-O-GlcNAc antibody). The lysate-RL2 mixtures were subjected to UV irradiation (365 nm). Next, the lysates were immunoprecipitated with protein G sepharose to enrich for O-GlcNAc-modified proteins. The immunoprecipitates were resolved by SDS-PAGE and probed by immunoblotting with anti-SP1 and anti-NUP153(SA1) antibodies. Both SP1 and NUP153 are known to be O-GlcNAc-modified and both proteins were efficiently immunoprecipitated in all conditions. For both SP1 and NUP153 immunoblots, higher molecular bands were observed only in those lanes corresponding to cells that had been transfected with pCMV6-XL5-AGX1 (F383G) and cultured with Ac₃GlcNDAz-1-P(Ac-SATE)₂. These higher molecular weight bands likely represent crosslinked complexes between RL2 and O-GlcNDAz-modified SP1 or NUP153. Alternatively, some of the bands may correspond to crosslinked complexes between endogenous proteins and O-GlcNDAz-modified SP1 or NUP153. Cotransfection with pCDNA4/TO/ncOGT-myc-His had no effect on crosslinking efficiency and was not conducted in other experiments.

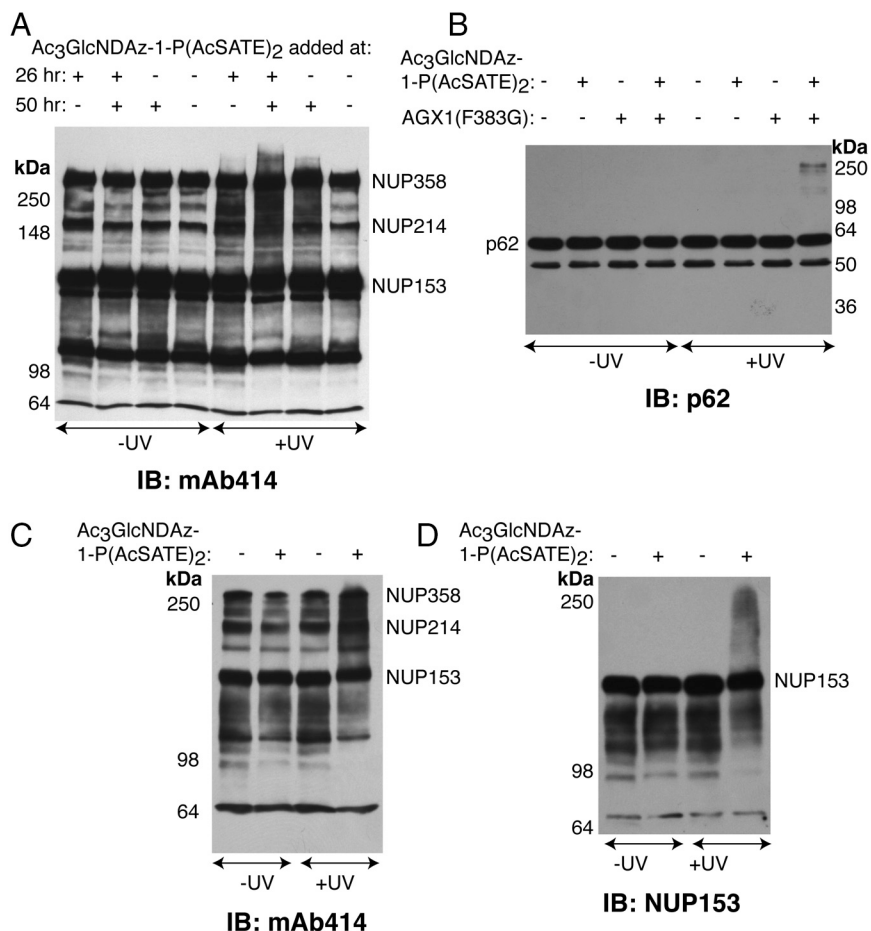


Fig. S5. Crosslinking of O-GlcNDAz-ylated proteins in intact cells. HeLa cells were transiently transfected with pCMV6-XL5-AGX1(F383G) and Ac₃GlcNDAz-1-P(Ac-SATE)₂ was added at the time(s) indicated (26 or 50 h after transfection). Cells were divided and half of each sample was irradiated with 365 nm light, prior to cell lysis. The lysates were analyzed by immunoblot using mAb414 (A). Normal HeLa cells or HeLa cells stably expressing AGX1(F383G) were treated twice with Ac₃GlcNDAz-1-P(Ac-SATE)₂ (at 0 and 24 h). Cells were divided and half of each sample was irradiated with 365 nm light, prior to cell lysis. The lysates were analyzed by immunoblot using an antibody recognizing NUP62 (B). T84 cells stably expressing AGX1(F383G) were cultured with Ac₃GlcNDAz-1-P(Ac-SATE)₂. The cells were divided and half of each sample was irradiated with 365 nm light, prior to cell lysis. The lysates were analyzed by immunoblot using mAb414 (C) or an antibody recognizing NUP153 (D).

Table S1. Tryptic peptides identified by MS/MS analysis of gel slices from crosslinked mAb414 immunoprecipitate (Fig. 4B, lane 2)

protein name	GI#	MASCOT score	peptide sequence	ion score
Region 1 of gel				
RanBP2 (NUP358)	1009337	1108	YIASVQGSTPSR	58
			SVELNPTQKDLVLK	30
			ELLQSFDSALQSVK	88
			SGQSALYDALFSSQSPK	55
			DTSFLGSDDIGNIDVR	52
			DTSFLGSDDIGNIDVR	45
			DTSFLGSDDIGNIDVREPELEDLTR	63
			LLVQHEINTLR	48
			IIDSDSNLSVVK	63
			NVSGISFTENMGSSQK	83
			APGTNVAMASNQAVR	81
			SDAGNLNFEFQVAK	60
			ELVGPPLAETVFTPK	72
			QNQTTSAVSTPASSETSK	44
			LHDSSGSQVGTGFK	59
			FGESTTGFNFSFK	57
			ERTDVIQGDDVADATSEVVSSTSETPK	35
			SNNSETSSVAQSGSESKVEPK	41
			SGEEDDEILFKER	80
			ITMELFSNIVPR	42
NUP214	33946327	336	SPGSTPTTPTSSQAPQK	43
			SAQGSSSPVPSMVQK	35
			TTLLEGFAGVEEAR	68
			ETLFNTLANNR	48
			LNHLVDSLQQLR	39
			QMASQAPAVNTLTESTLK	67
			NVPQVVNVQELK	40
exportin-1 (CRM1)	4507943	127	LLSEEVDFDSSGQITQVK	57
			EPEVLSTMAIIVNK	32
			EFAGEDTSDLFLEER	43
transportin-1 (TNPO1)	133925811	92	GDVEEDETIPDSEQDIRPR	37
			TLENTAITIGR	55
Karyopherin β 1 (importin subunit β 1)	119615215	81	LAATNALLNSLEFTK	71
NUP153	31418202	52	IPSIVSSPLNSPLDR	54
Region 2 of gel				
RanBP2 (NUP358)	1009337	373	DVQESRELLQSFDSALQSVK	25
			ELLQSFDSALQSVK	79
			SLGGNDELSATFLEMK	22
			IIDSDSNLSVVK	61
			ELVGPPLAETVFTPK	66
			FGESTTGFNFSFK	33
			SNNSETSSVAQSGSESKVEPK	27
			ITMELFSNIVPR	35
NUP214	119608367	192	SPGSTPTTPTSSQAPQK	25
			TTLLEGFAGVEEAR	53
			ETLFNTLANNR	55
			NVPQVVNVQELK	30
NUP153	31418202	72	IPSIVSSPLNSPLDR	67
transportin-1 (TNPO1)	133925811	70	GDVEEDETIPDSEQDIRPR	20
			TLENTAITIGR	44
nuclear RNA export factor 1 (NXF1)	4406524	67	AQFFVEDASTASALK	62
exportin-1 (CRM1)	4507943	58	EPEVLSTMAIIVNK	20
			EFAGEDTSDLFLEER	35
gamma-catenin	29650759	57	ALMGSPQLVAAVVR	28
karyopherin β 1 (importin subunit β 1)	19923142	21	AAVENLPTFLVELSR	41
Region 3 of gel				
RanBP2 (NUP358)	1009337	412	ELLQSFDSALQSVK	71
			SGQSALYDALFSSQSPK	32
			DTSFLGSDDIGNIDVR	56
			ELVGPPLAETVFTPK	64
			LHDSSGSQVGTGFK	38
			FGESTTGFNFSFK	40
			ERTDVIQGDDVADATSEVVSSTSETPK	37
			SGEEDDEILFKER	30
NUP214	119608367	168	SAQGSSSPVPSMVQK	21
			TTLLEGFAGVEEAR	49
			LNHLVDSLQQLR	40
			QMASQAPAVNTLTESTLK	50

protein name	GI#	MASCOT score	peptide sequence	ion score
NUP153	31418202	72	IPSIVSSPLNSPLDR	56
			FVASKPLEEEEMEVPVLPK	20
			SSFNLGTIETK	37
			NVFSSSGTSFSGR	56
Region 4 of gel				
RanBP2 (NUP358)	1009337	800	ELLQSFDSALQSVK	55
			DTSFLGSDDIGNIDVR	42
			DTSFLGSDDIGNIDVREPELEDLTR	67
			LLVQHEINTLR	51
			TGSGLNSFYDQR	29
			IIDDSDSNLSVVK	74
			APGTNVAMASNQAVR	77
			SDAGNLNFEFQVAK	42
			ELVGPPLAETVFTP	78
			GVIFGQTSSTFTFADLAK	41
			FGESTTGFNFSFK	67
			ERTDVIQGDDVADATSEVEVSSTSETTPK	43
			TDVIQGDDVADATSEVEVSSTSETTPK	21
			ITMELFSNIVPR	58
			ITMELFSNIVPRTAENFR	41
			NUP153	31418202
SSFNLGTIETK	43			
NVFSSSGTSFSGR	61			
NUP214	119608369	111	QMASQAPAVNTLTTESTLK	22
			NVPQVVNVQELK	42
histone H2B	1568551	51	AMGIMNSFVNDIFER	54
myomesin 1	119622088	51	IIPSR	26